USING NUTRIENTS, SEDIMENT, IONS, ISOTOPES, AND HYDROGRAPH SEPARATION TO QUANTIFY CONDUIT-DOMINATED RECHARGE PROCESSES IN A TRINITY AQUIFER SITE: CAVE WITHOUT A NAME

by

Michael S. Markowski, B.S.

A thesis submitted to the Graduate Council of
Texas State University in partial fulfillment
of the requirements for the degree of
Master of Science
with a Major in Aquatic Resources
May 2016

Committee Members:

Benjamin F. Schwartz, Chair

Weston H. Nowlin

Astrid N. Schwalb

FAIR USE AND AUTHOR'S PERMISSION STATEMENT

Fair Use

Duplicate Permission

ACKNOWLEDGEMENTS

I thank my advisor, Dr. Benjamin Schwartz, for sharing his knowledge and experience and for his commitment to me over the last three years. I thank my committee members, Dr. Weston Nowlin and Dr. Astrid Schwalb, for their insight and contributions to this work. I thank the entire staff at CWAN, especially owner, Tom Summers, and manager, Mike Burrell, for granting access and supporting research at Cave Without a Name. I thank Gabrielle Timmins for the hours of work and assistance in the lab. I also thank my brother Steven Markowski, Aaron Swink, Amelia Everett, Nate Trimble, and Tom Heard for their assistance in the field and lab. I thank the Karst Waters Institute for partial funding of this work.

TABLE OF CONTENTS

Page

LIST OF TABLES

Table **Page**

LIST OF FIGURES

Figure **Page**

ABSTRACT

Cave streams provide an ideal location for sampling waters transported through a karst system because they integrate basin-wide sources ranging from fast flow in conduits to slow flow through the bedrock matrix. Although numerous studies have monitored cave streams to characterize these process, most have infrequent sampling intervals and/or a limited number of measured parameters. This study used a large dataset that includes high frequency sampling and comprehensive stormwater analyses of surface and cave stream water from five storm events between July 2014 and July 2015 at Cave Without A Name (CWAN) in central Texas. The objectives were to 1) determine which environmental factors influence the timing and proportions of stormwater and pre-event water moving through the system and 2) to quantify relationships between discharge and sediment, nutrient, and ion concentrations within and across storm events. Results show that evapotranspiration (summed over prior 12 weeks to each storm), soil moisture (at 10-40cm), and cave-stream discharge prior to each storm affects the timing of the peak ratio of stormwater/pre-event water flow through the cave. As antecedent conditions became wetter from July 2014 to July 2015, peak stormwater arrival times dropped from days to hours. Progressively faster stormwater arrival times, heterogeneity within and across storm chemographs and sediment graphs, and water isotope data all indicate a flushing of accumulated solutes in the upper

unsaturated zone during Events 1 and 2, and progressive wetting of unsaturated portions of the system from July 2014 to July 2015. Taken together, these data reveal complex hydrologic and mass transport dynamics, variable rainfall-runoff and rainfall-recharge relationships, and highlight that a single storm cannot be used to accurately describe how a karstic groundwater system responds to storm events under a wide range of hydrologic conditions. These data may also help explain inconstancies between findings from other studies in which contaminant or nutrient concentrations varied from storm-to-storm. This better understanding of recharge processes at CWAN will help guide future research on transport dynamics in karst systems, as well as contribute to better surface water/groundwater management in karst regions.

I. INTRODUCTION

As surface water infiltrates and moves down through the unsaturated zone it transports natural tracers including sediment, nutrients, cations, and anions. These waters also have event-specific characteristics such as liquid water stable isotope ratios, temperature, specific conductivity, and pH. In karst settings, cave stream and karst springs are useful sites for monitoring and sampling infiltrating water and tracers, as these sites integrate both slow moving matrix water and fast conduit flows. Cave streams and karst springs thus have the potential to serve as a source of information that can be used to determine basin-scale hydrogeologic responses, as well as to quantify the dynamics of natural tracers (nutrients, ions, and sediment) as they are transported through a system.

For decades, scientists have recognized that storm events play an ecological, geomorphic, and speleogenetic role in moving water and materials through karst systems as they induce sudden and transient changes in the relatively stable karst subsurface (Hawes 1939). Studies have measured and monitored natural environmental tracers to provide insights into the timing, quantity, and quality of water entering, cycling through, and leaving karst systems. Shuster and White (1971) sampled for Mg^{2+}/Ca^{2+} ratios, temperature, hardness, and pH every two weeks for one year to group 14 springs into conduit dominated vs matrix dominated springs. Martin and Dean (1999) used temperature data collected at 90-second intervals to calculate the fluctuations in the short residence times in Florida karst aquifers. More recently, in a study that utilized high frequency sampling of waters during storm events, Toran and Reisch (2012) analyzed Mg^{2+}/Ca^{2+} ratios at 30 minute intervals for 12 hours during four separate storm events.

These data suggested heterogeneity in timing and volume of stormwater vs pre-event water both within and across the four events arriving at a single spring discharge point.

Because karst systems have the potential to evolve rapidly in response to large storm events there is a need to understand how different natural tracers enter, move through, and exit the system at fine time scales. Previous studies have been limited to a small number of tracers (Toran and Reisch 2012; Martin and Dean 1999) and/or infrequent sampling intervals (Shuster and White 1971). Utilizing a large number of water quality parameters at more frequent time scales is required to more fully understand storm responses in karst systems. This necessity is due to the fact that the movement of water and natural tracers are controlled by dynamic environmental factors that may change considerably over short time scales within a single event (Toran and Reisch 2012). A few recent studies have used multiple tracers at short (1 hour or less) time intervals in various karst settings (Cholet et al. 2015; Yang et al. 2013; Mudarra et al. 2013; Vanderhoff 2011).

Periodic grab samples for $\delta^{18}O$ and $\delta^{2}H$ stable isotopes and ions were collected at each site during two previous storm events to build a preliminary dataset (Gerard 2012). Prior work from this study and Schwartz et al. (2013) suggest that a combination of precipitation, antecedent soil moisture, potential evapotranspiration (PET), and vegetation cover above the cave can be used to predict the response at in-cave sites, and that these responses vary after different magnitude precipitation events. However, relatively infrequent water sampling limited the ability of prior work to understand detailed interactions between suspended and dissolved loads and the proportions of event

water and pre-event water across rapidly evolving storm hydrographs under varying antecedent conditions.

Past studies that monitored a large number of natural tracers in karst systems have distinguished between ionic tracers sourced from local carbonates and those sourced in the soil (Yang et al. 2013; Cholet et al. 2015; Mudarra et al. 2013). Ions such as Ca^{2+}, Mg^{2+}, Sr^{2+}, HCO^{3-} and SO_4^{2-} mainly result from the dissolution of local carbonates, but may also be derived from soil weathering. Tracers including NO_3^-, Cl^-, K^+, Na^+, and PO_4^{3-} are deposited atmospherically or have local anthropogenic sources in settings similar to CWAN, and can be further concentrated in the soil by evapotranspiration. Also, in the soil, NO_3^- is produced from the biological fixation of atmospheric N_2 and dissolved organic carbon (DOC) is sourced from the incomplete degradation of organic matter. In similar systems, total suspended solids (TSS) and non-volatile suspended solids (NVSS) have been shown to be both a combination of autochthonous and allochthonous sediment (Fournier et al. 2007; Massei et al. 2003; Pronk et al. 2009; Goldscheider et al. 2010; Mahler and Lynch 1999). $\delta^{18}O$ and δ^2H ratios in precipitation can change over single rain events (Dansguard 1964) and have different seasonal variations (Blavoux 1978).

In addition to having spatially distinct sources that may vary in concentration episodically or seasonally, different natural tracers behave as conservative or non-conservative. Under oxidizing conditions generally present in unsaturated zones of upland karst systems, DOC is considered as a non-conservative tracer as it quickly mineralizes into inorganic carbon within a few weeks (Batiot 2002; Ford and Williams 2007). Under similar conditions, Ca^{2+} and specific conductivity (SC) can only be

considered conservative for 12 to 24 hours following rainfall due to calcite dissolution kinetics (Mahler and Garner 2009). NO_3^- is conservative under the same oxidizing conditions (Perrin et al. 2007). All anions and Mg^{2+} are considered conservative for time scales in this study. $\delta^{18}O$ and $\delta^{2}H$ ratios do not change due to reactions in the subsurface but are susceptible to fractionation caused by evapotranspiration near the surface.

The purpose of this study was to determine the factors which influence the timing and quantity of stormwater and pre-event water, and the dissolved and particulate loads that are carried by stormwaters, as a storm hydrograph moves through a karst system. This study was also designed to quantify changes in and relationships between nutrients, dissolved ions, sediment, and liquid water stable isotopes across multiple storm hydrographs, and to determine how the loadings of these parameters vary across multiple storm events.

I predicted that:

1) Antecedent conditions and rainfall amount would control the timing and quantity of stormwater and pre-event water that moves through a cave stream. Wetter antecedent conditions and higher rainfall magnitudes should cause higher amounts of stormwater to move through the system faster than under dry antecedent conditions.
2) Assuming the system is nutrient limited and that nutrient uptake rates are relatively slow, peak concentrations of nutrients (P, N, and C) will coincide with peaks in stormwater flushing though the system. This flushing will also coincide with low concentrations of cations and anions.

3) I also predicted that sediment concentrations moving through the system will primarily be from remobilization of sediment in conduits during peak discharge, rather than import of new sediment from the surface, and that these concentrations will consist of primarily of non-volatile suspended sediment, rather than organic detritus imported from the surface.

*II. M*ETHODS

Study Site

Cave Without A Name (CWAN) (29°53´10.88N, 98°37´02.78W) is a commercial cave located about 35 km northwest of San Antonio, Texas and near the southern extent of the Trinity Aquifer where average yearly rainfall since 1885 is 737 mm. (NOAA 2012). CWAN offers easy access to a large stream conduit and several drip-sites and is owned by an individual who encourages scientific study of the cave. Due to its location and the fact that the stream integrates discharge from a relatively large area, CWAN is an ideal environment in which to study infiltration and recharge processes. The known cave is an active branchwork stream that lies 20-50 m below the surface and likely began forming approximately 880 ka B.P. in the Lower Glen Rose Formation of the Trinity Group (Veni 1994).

The Trinity Aquifer in Central Texas is a regionally extensive Cretaceous carbonate aquifer of more than 200,000 km^2 and stretches from the northwestern boundary of the Balcones Fault Zone from southern Oklahoma and Arkansas to West Texas (Ryder 1996) (Figure 1). The Trinity Aquifer is also a main source of water for residents on the Edwards Plateau, where surface streams are uncommon and fed almost exclusively by karst spring discharges during baseflow conditions. Rapid population growth in this region and increasing groundwater extraction have recently caused conflicts over groundwater use and have highlighted how little we know about the Trinity Aquifer (Mace 2000).

Data Collection

At CWAN, continuous data have been collected at 10-minute intervals since 2009 at five sites in the cave and at one surface site above the cave. At the main cave stream

(Main Stream) a CTD Diver data logger (Schlumberger Limited, Tucson, AZ, USA) recorded pressure, temperature, and conductivity at 10 minute intervals. An adjacent barometric pressure logger (Schlumberger Limited, Tucson, AZ, USA) was used to calculate stage at the Main Stream site and a small v-notch weir allows discharge to be measured during low-flow conditions and estimated during flood-discharges.

Other in-cave sites where data are collected but not used in my study include an ephemeral spring (Rimstone Spring), equipped with a CTD Diver, and three speleothem drip sites (White Grapes, Last Switch, and Near Stream) (Figure 2). At the drip sites a small plastic tarp collects and funnels water to a tipping bucket rain gauge that logs drip rate via a micro-station data logger (HOBO H21-002, ONSET Computer Corp, Bourne, MA, USA). Water temperature and SC data are collected using a Conductivity/Temperature Data Logger (HOBO U24-001 ONSET Computer Corp, Bourne, MA, USA) situated in a collection cup on top of the rain gauge.

A weather station (HOBO H21-001) records meteorological data adjacent to the cave's entrance, including precipitation, temperature, barometric pressure, solar radiation, and wind speed and direction at ten minute intervals. A direct recharge site on the surface, called Joe's Diet Cave, is a vertical shaft cave entrance and is located in a roadside drainage ditch several hundred meters from the CWAN entrance. During storms that cause runoff, nearly all the water in the ditch flows directly into the cave entrance. The site was used as a collection site for recharging stormwaters that are assumed to drain into CWAN (to-date, no dye-trace has confirmed this connection, though proximity to a known tributary passages in the cave suggests that this is a direct recharge point for waters entering CWAN).

High frequency water sampling at the main cave stream and at the surface runoff/direct recharge site was carried out during and after five storm events. Discrete water samples were collected using an automated water sample collector (ISCO 6700 Series Water Sampler) at Main Stream and at Joe's Diet Cave. Water samples were collected at varying intervals at each site, with higher frequency during the rising limb and peak of the hydrographs. Sampling intervals for sequential sampling across a storm hydrograph in Main Steam were typically as follows: the first sample was collected at the initial rise in stream stage, 6 samples thereafter at 5-minute intervals, then 6 samples at 15-minute intervals, then 6 samples at 30-minute intervals, then 18 samples at 60-minute intervals, then 12 samples at-2 hour intervals, then 24 samples at 6-hour intervals, and then 24 samples at 12-hour intervals. Extended sampling was performed on the fifth storm event, and samples continued to be collected at either 12-hour intervals, or 24-hour intervals. Sampling duration at Joe's Diet cave varied depending on the available surface runoff, but samples were collected across the run-off hydrographs at intervals similar to the Main Stream site. Direct discharge measurements were taken in Main Stream and adjacent to Joe's Diet Cave at different stream stages to establish stage-discharge rating curves to relate stream stage to discharge. Precipitation samples were collected using a collector that minimizes evaporation at the weather station rain gauge, and periodically from a bucket during and immediately after each storm event. Events 1 and 4 lack surface runoff samples and precipitation samples because no one was present at the CWAN site during these two storms.

After collection, water samples were placed on ice and transported to the lab as soon as possible. Each water sample was processed using established methods. Samples

analyzed for isotopes, ions, and dissolved nutrients were filtered in the lab with Pall A/E (1µm nominal pore size) ashed filters. Both dissolved nutrient samples and total nutrient samples were preserved with H_2SO_4 and stored in 125 mL high-density polyethylene (HDPE) bottles and refrigerated. Water samples for analysis of liquid water stable isotopes ($\delta^{18}O$ and $\delta^{2}H$) and ions were filtered and stored in 60 mL HDPE bottles and refrigerated. Separate 40 mL glass vials were used to hold filtered water samples for analysis of DOC.

Liquid water stable isotopes, major ions, TSS, NVSS, and nutrient concentrations were measured for each sample in-house in Dr. Schwartz's lab at Texas State University. Liquid water stable isotopes were analyzed using a Los Gatos Research DLT 100 Liquid Water Isotope Analyzer (Los Gatos Research, Inc., Mountain View, CA, USA). Major ions were analyzed with a Dionex ICS 1600 Liquid Ion Chromatographs (Thermo Fischer Scientific, Walther, MA, USA). Total Phosphorus (TP) and soluble reactive phosphorus (SRP) concentrations were determined utilizing the ascorbic acid method (Wetzel and Likens 2000). Total nitrogen (TN) and nitrate (NO_3^--N) were determined using second-derivative spectroscopy on a Varian Cary 50 UV/VIS Spectrophotometer (Crumpton et al. 1992). Ammonium was determined using methods modified from the phenate method (Wetzel and Likens 2000). Total suspended solids (TSS) and total nonvolatile suspended solids (NVSS) were determined by weighing the dried (at 50°C) and muffled (550°C) Pall A/E filters and taking into account volume of water filtered. (Standard Methods Online 2012).

Initial spikes in nutrient data over the first few samples, especially in DOC and TP, were suspiciously high, often 10x that of background levels, and occurred well before

the event-water arrival. I suspected that these anomalous values resulted from biofilm buildup inside the intake hose of the ISCO. To test this hypothesis in the field, I performed an experiment in which the ISCO autosampler that was still deployed in the field was also used to collect Milli-Q deionized water for six one-liter samples. The expectation was that nutrient levels in the DI samples would be high if they resulted from biofilm accumulations, rather than an initial pulse of nutrients in the conduit water. The resulting analyses confirmed that these initial spikes in nutrients were artifacts – and most likely were the result of biofilms building up in the ISCO sampling tube – and that initial spikes in nutrients did not represent actual nutrient levels in the stream waters. I am unaware of any previous studies that have addressed this specific problem of contamination buildup in permanent sampling setups over time, although a few studies have attempted for to quantify contamination between samples (Robert and Eads 1983).

Data Analysis

A two end-member hydrograph separation analysis was performed for the five storm events using both $\delta^{18}O$ and Mg^{2+}. $\delta^{18}O$ and Mg^{2+} were selected since both are considered stable over the time scale of days to weeks in an underground oxidizing environment similar to CWAN. Mg^{2+} end-member models were used in the final analysis because $\delta^{18}O$ values in rainfall and runoff samples varied greatly within single storm events and also the majority of water samples collected had $\delta^{18}O$ values outside the range of the two established $\delta^{18}O$ endmembers for each event. Mg^{2+} and $\delta^{18}O$ concentrations in surface runoff entering the direct recharge site and in pre-event water from Main Stream were used as stormwater and pre-event water end-members, respectively. Discharge

weighted Mg^{2+} averages of 11-12 samples were used to establish one surface runoff end-member per storm event (Equation 1).

$$Mg_{\text{wavg}} = \frac{\sum_{i=1}^{n} MgiPi}{\sum_{i=1}^{n} Pi} \quad (1)$$

Mgi is the concentration of Mg^{2+} (or $\delta^{18}O$) at the i^{th} sample, Pi is the sum of runoff of the ith sample, n is the number of samples used, and Mg_{wavg} is the discharge weighted average of samples. At the beginning of an increase in stage resulting from a storm event, the first ISCO sample collected at the Main Stream site, or a manual sample collected just prior to an increase in stage, was used to establish a pre-event end-member magnesium concentration or stable isotope ratio.

The following (Equation 2) was used to separate the hydrograph at Main Stream, using the two end-members defined above.

$$Qe = Qt\frac{Cs-Cpe}{Ce-Cpe} \quad (2)$$

Q_e is the stage of event water in Main Stream, Q_t is the total volume of water at Main Stream, C_s is the tracer (Mg^{2+} or $\delta^{18}O$) concentration of Main Stream at a given time, C_{pe} is the pre-event tracer concentration in Main Stream, and C_e is the event surface runoff water tracer concentration.

Hysteresis plots of different tracers at Main Stream were used to understand in more detail how the system responds to storm events. Hysteresis plots can be used to visualize changes in tracer concentrations at different points along a hydrograph. Toran and Reisch (2013) used hysteresis plots of Mg^{2+}/Ca^{2+} ratios to infer different source-waters in a spring both within and between storm events.

Statistical Analysis

Statistical analyses were performed using the program, R (R Core Team 2015). Relationships between multiple environmental predictors (PET, soil moisture, pre-event stage) and rainfall characteristics (rainfall intensity, rainfall duration, rainfall amount) were used to predict timing of maximum event/pre-event water ratios and maximum and minimum tracer concentrations in Main Stream. A Pearson r value was calculated for each linear combination of variables using a correlation matrix. An ordinary least-squares linear regression was used to assess the influence of difference environmental variables and rainfall characteristics on Main Stream response variables. Logarithmic regressions were also used when appropriate to describe several relationships.

Potential evapotranspiration values were determined using the Penman-Monteith equation with a short grass (Allen 2005). Because of on-site sensor failure and insufficient funds to replace them, soil moisture data were obtained online from the Goddard Earth Sciences Data and Information Services Center (NASA 2015). A LOESS smoothing function (α=0.33) was applied to smooth the TSS and NVSS data. This function is a locally weighted polynomial regression that uses weighted least squares fitting (Cleveland and Devlin 1988). Once smoothed, the data were used to obtain times of maximum sediment concentrations prior to running statistical analysis.

III. RESULTS

Precipitation and Hydrographs

From July 17, 2014 to July 18, 2015 five major rain events (Events 1-5) of similar magnitude (43.9-72.6 mm) caused responses at Main Stream in CWAN. The five events occurred during different times of the year and under different antecedent conditions. Events 1-4 resulted from single precipitation events of varying intensity lasting from < h to > 24 h in length. Event 5 is comprised of an initial event of 48 hours followed by 7 additional responses that occurred consecutively during an 18 day period with a cumulative total of 330 mm of rainfall (Figure 3). Because the automated water sample collector failed to initiate sampling properly in Event 4 sampling began about 6 hours after the initial response in Main Stream and sampling was discontinued after only 48 hours. Event 4 data also does not include dissolved or total nutrients or sediment.

Prior to the first rain event, and due to a multi-year cumulative precipitation deficit in precipitation, hydrologic drought conditions existed at the cave site. During the 366 day study period (July 17, 2014- July, 18 2014) 934.2 mm of precipitation was recorded at the surface weather station. During each event, the Main Stream stage increased from baseflow conditions of 2.7 cm (prior to Event 1) to 6.1 cm (prior to Event 5) and stage peaks ranging from 25.3 cm (Event 1) to 88.7 cm during the first peak of Event 5. Subsequent stage peaks during the prolonged Event 5 reached up to 260.0 cm.

Hydrograph Separation

All events showed no event water during the initial portion of the rising limb of the hydrograph. After the initial pulse of pre-event water, event water arrived and geochemical and thermal changes occurred. The initial pulse of older water is

characterized by event water values of less than 0% (Figure 4). Maximum event-water contributions varied from 47.1% during Event 1 to 82.0% during Event 5 and occurred at after a maximum of 113.3 hours (Event 2) and minimum of 9.4 hours (Event 5) after initial stage rise. For all events, event-water contributions remained through the sampling period.

Sediment

Figure 5 shows TSS, NVSS, and stage at Main Stream. The timing of peak sediment concentration relative to maximum discharge varies across events. TSS and NVSS peaks arrive after (Event 1, 2), during (Event 3), and before (Event 5) Main Stream peak stage. TSS and NVSS peaks arrive before peak stormwater/pre-event water ratios in all events. Peak sediment concentrations vary significantly across events. Event 2 has peak TSS and NVSS concentrations of 3.03 mg/L and 1.89 mg/L while Event 5 has TSS and NVSS peaks of 32.07mg/L and 26.59mg/L.

Nutrients

TP and SRP (Figure 6), TN and NO_3^- (Figure 7), and DOC and NH_4^+ (Figure 8) are plotted in time series for Events 1, 2, 3, and 5. For all storm events, DOC responded with an overall increase and then recovery towards the background DOC concentration of ~1.0 mg/L. Events 1, 2, 3 had similar DOC peak concentrations of ~5.0 mg/L; Event 5 had a peak concentration of 7.8mg/L. DOC peaks appeared to be closely associated with peaks in maximum event-/pre-event water ratios at Main Stream. DOC peaks occur after peak stage in Events 1-3 and coincide with peak stage in Event 5. As with peaks in event/pre-event water ratio arrivals, DOC peaks also occurred earlier with each subsequent storm event, peaking in 113.73 hours after initial Main Stream stage rise in

Event 1 and only 9.0 hours after initial rise in Event 5. Background TP concentrations for all storm events were low (<10µg/L). Similar to DOC, TP concentrations generally peak earlier with each subsequent event, from 36.06 and 42.67 hours in Event 1 and 2 respectively, to 6.0 hours in Event 5. SRP concentrations in general followed the same patterns as TP.

TN, NO_3^-, and NH_4 concentrations showed different patterns across storm events. Events 3 and 5 showed the inverse behavior of DOC and TP. After an initial lag and increase in concentration, TN and NO_3^- decreased, reached a minimum, and later gradually recovered to near pre-event concentrations. Event 1 and 2 initially had small dips followed by small peaks and a subsequent return to background concentrations. A much later delayed decrease in TN and NO_3^- occurred in Event 1 was likely the result of additional rainfall. Most of the nitrogen cycling through CWAN was in the form of NO_3^-, but mean ratios of TN to NO_3^- within storm events did vary: the minimum was 1.05 during Event 2 and the maximum was 1.34 during Event 3.

Temperature and Specific Conductivity

Temperature signals were distinct across events (Figure 9). Temperature initially decreased and then recovered in Events 1 and 2. During Event 3 temperature initially increased and then had a larger decrease and recovery. Event 4 temperature initially decreased and then had a larger increase and recovery. Event 5 had a small initial increase and larger decrease and recovery for the first storm. The next two responses in Event 5 had overall decreases and the final five responses had overall increases and recoveries. The arrival times of temperature maximum/minimum concentrations varied greatly relative to other tracers. Temperature maximum occurred before any other tracer

maximum/minimum concentration in Event 2 and temperature was the last tracer in Event 5 to show a maximum or minimum.

Overall, conductivity responses were similar across events (Figure 9). For each event there was an initial rise followed by a large dilution curve and recovery. The time between initial rises in a hydrograph and the conductivity minimums varied from over 6 days during Event 2 to only 8 hours for Event 5. Conductivity minimums happened after temperature minimums for Events 2 to 5 and before temperature maximums in Events 1 and 2.

Ions

The behavior of ions across the five event hydrographs can be placed into two general categories. Ca^{2+}, Mg^{2+}, F^{-}, and K^{+} all showed overall concentration dilutions and subsequent recoveries during all five events. Cl^{-}, Na^{+}, NO_3^{-}, and SO_4^{2-} show overall concentration dilutions for Events 3-5, and only small decreases or increases of concentration for Events 1 and 2. Two hysteresis plots show Mg^{2+} and Na^{+} plotted with stage (Figure 10). Event 4 was excluded due to the incomplete data across the hydrograph. The hysteresis plot of Mg^{2+} showed that Mg^{2+} concentrations change in a uniform way but at different times of the hydrograph. For example concentrations increased initially, decreased and then slowly recovered. Minimum Mg^{2+} concentrations occurred from the tail end of the hydrograph when stage had returned to near baseflow conditions (Event 1 and 2) to the peak of the hydrograph in Event 5.

The hysteresis plot of Na^{+} shows two types of responses. Events 1 and 2 showed overlap in Na concentrations on the rising and falling limb of the stage curve. Event 2 has

multiple figure eight loops. Event 3 and the first response of Event 5 show single loops similar to the Mg^{2+} loops.

Isotopes

Time series $\delta^{18}O$ and $\delta^{2}H$ data at Main Steam for Events 1, 2, 3, and 5 are shown in Figure 11 and Figure 12 respectively with the units per mil (‰) deviations relative to Vienna Standard Mean Ocean Water (VSMOW). Pre-event background levels of $\delta^{18}O$ in Main Stream are similar to the observed long term local weighted precipitation average (-4.1‰) by Pape et al. (2010) from 1999-2007 in Austin, Texas. Table 3. Range of δ2H and δ18O ratios in Main Stream (left) and surface runoff (right) for Events 1, 2, 3, and 5.summarizes the ranges of $\delta^{18}O$ and $\delta^{2}H$ ratios observed in Main Stream for Events 1, 2, 3, and 5. These ranges for a single event increase with successive events with the exception of $\delta^{18}O$ ratios between Events 1 and 2.

Figure 13 and Figure 14 show both the data at the surface recharge site and Main Stream plotted with the Global Meteoric Water Line (GMWL) represented by $\delta^{2}H = 8\delta^{18}O + 10$. To provide a sense of changes through time, the data points were given a size weight with the first data point and last data point from each event having the smallest and largest points on the graph respectively. Figure 14 shows the clustering of isotope values decreased with successive events. Events 1, 3, and 5 have data points that plot beneath the GMWL. This is indicative of an evaporative fractionation of $\delta^{18}O/\delta^{2}H$ ratios. All of these points that plot beneath the GMWL in Event 3 are immediately following a secondary smaller rain event. In Event 2 these points of enriched isotope ratios are following a secondary smaller rain event with the exception of a few at the onset of the event. In Event 5 all of these enriched points are at the very start of the event.

Two endmember mixing models using $\delta^{18}O$ were not effective at predicting event/pre-event water ratios. One limitation of these models was the wide range in values of $\delta^{18}O$ in runoff waters. For example in Events 2, 3, and 5, $\delta^{18}O$ values in surface runoff are were well above and below the background levels recorded at Main Steam prior to each storm. Using a volume weighted surface runoff value for $\delta^{18}O$ in a two end member mixing model indicated no event water reached Main Stream in Event 3. The model suggested only 15 samples of any event with and maximum event water contribution at Main Stream of 4.1% in Event 2. The $\delta^{18}O$ mixing model for Event 5 had a maximum event water contribution of 48.2% compared to 82.0% with the Mg^{2+} model. Comparing the two ratios of event/pre-event water over the entire hydrograph for the Mg^{2+} model against the $\delta^{18}O$ model gave an R^2 value of only 0.33.

Comparing tracer responses

Response times for tracer maximum and minimum concentrations at Main Stream in Events 1 and 2 are generally much slower, often >10x that of Events 3-5, and tracer concentration and dilution curves are flashier in Events 3-5. Some tracers (Ca^{2+}, Mg^{2+} DOC, TSS, NVSS and SC) show consistent overall patterns across all storm events, while other tracers (NO_3^-, Na^+, Cl^-, and SO_4^{2-}, $\delta^{18}O$, δ^2H, and temperature) have responses that are not generally consistent across events. For example, during the first two events, ions that are not sourced from the dissolution of carbonate rock (NO_3^-, Na^+, Cl^-, and SO_4^{2-}) showed both small concentration increases and dilutions of ions over the storm hydrographs. In Events 3-5 these same ions showed one large dilution in concentration followed by a recovery to the background levels. Ions sourced from the dissolution of the local carbonates (Ca^{2+} and Mg^{2+}) showed an overall dilution and recovery during all five

storm events. Similarly, DOC also showed a general concentration and recovery during all five storm events (Figure 1. Location of CWAN (blue dot) relative to the Trinity Formation (modified from Clarke et al. 2014).

Relationship between parameters

Soil moisture, cumulative 12 week PET total, and pre-event stage at Main Stream were statistically significant predictors of the timing of peak stormwater/pre-event water ratios at Main Stream based on Mg^{2+} ion hydrograph separation analysis. The timing of minimum Mg^{2+} ion concentration had a significant linear relationship ($p<0.05$) with PET. The timing of minimum Mg^{2+} ion concentration and had a logarithmic relationship with both pre-event stage and soil moisture (Figure 15. Relationships between various environmental parameters across the five storm events..

Timing of minimum conductivity and pre-event stage also had a logarithmic relationship. A least squares linear regression indicates two predictor variables, soil moisture and pre-event stage, had a significant linear correlation. Rainfall total and average rainfall intensity were not significant in describing stormwater and pre-event water at Main Stream. Rainfall duration was significantly correlated with the timing of total peak stage ($p<0.05$) Figure 15.

I hypothesized that TSS and NVSS concentrations were both controlled by the total discharge of Main Stream. The timing of TSS and NVSS peaks had significant linear correlation with the timing of conductivity minimums ($p<0.05$) (Figure 15). Contrary to my hypothesis, no significant correlations were found between the timing and magnitude of TSS and NVSS peaks and Main Stream discharge.

The minimum concentration of Mg^{2+} and the maximum DOC and TP concentrations were all significantly correlated with each other ($p<0.05$). Figure 16 shows the relationship of different tracers for each storm event. These data are summarized in Table 3, which shows the timing and order of arrival of different tracers.

IV. DICUSSION

It was predicted that rainfall magnitude and antecedent conditions would control the timing and quantity of stormwater and pre-event water that moved through CWAN. Previous work showed that both antecedent conditions (Mudarra et al. 2013; Polk et al. 2013; Wong et al. 2012) and rainfall magnitude (Mudarra et al. 2013; Savoy et al. 2011) can affect the timing and amount of stormwater versus pre-event water moving through a karst system after a storm event. In this study, 12 month prior cumulative PET measured at the surface, soil moisture at 10-40 cm depth, and the Main Stream's pre-event stage were all significant predictors in the timing of maximum event water/pre-event water ratios in Main Stream. The significance of these environmental factors to the timing of event water and pre-event water moving through CWAN, as well as analysis of the variation in dissolved and particulate loads in Main Steam within and across storm events suggests: 1) a change in storage components and flow paths across storm events and 2) changing tracer source concentrations across events.

Storage components and flow paths

As antecedent conditions became wetter, data from this study suggests a threshold was reached after Event 2 where event water began to move through CWAN over hours rather than days. Successively decreasing event/pre-event water ratio lag times in Main Stream across Events 1-5 (108, 113, 16, 11, and 9 h) may be explained by shifting flow paths from different storage components as antecedent conditions progressed out of drought conditions. Perrin et al. (2003) proposed a conceptual model of karst system storage in the soil, epikarst, unsaturated, and phreatic zone. After a specific wetting threshold is reached water can bypass the soil and epikarst storage units and infiltrate

more rapidly through open conduits and factures. The fact that there were similar rainfall magnitudes and different rainfall intensities for Events 1-5, and that these factors showed no significant control on event water/pre-event water ratio time lags further suggests it is the antecedent conditions that primarily control event water and pre-event timing moving through CWAN.

At Main Stream peak event/pre-event water ratios occur closer to the peak in total discharge in later events. Compared to peak discharge, peak event/pre-event water ratios lagged by 103, 96, 9, 26, and 0.4 hours for Events 1-5. Not only is the stormwater arriving at Main Stream sooner in Events 3-5, but more stormwater volume is arriving as its peak concentration nearly coincides with the peak in overall discharge. Main Stream stage was back to baseflow levels in Events 1 and 2 when maximum event/pre-event contribution occurred, which suggests that more stormwater in Events 1 and 2 was stored in the soil, epikarst, and even in low gradient conduits (pools) instead of being transmitted to the monitoring site, while in Events 3-5 more event water bypassed these already wetted storage compartments and contributed more event water during the stage rise in Main Stream.

The flashiness of storm hydrographs and chemographs of karst springs has been understood to suggest how the system is conduit vs matrix dominated (Shuster and White 1972; Dreiss 1982; White 1988). In this study the general increased flashiness of the chemographs indicate a more conduit dominated system in the latter events. For example DOC peaks about 114, 71, 13, and 9 hours after the initial stage rise for Events 1-5 respectively. The recovery curves of DOC are steeper with each successive event (Figure 8). Similar trends are in most tracers. Mg^{2+} minimums occur about 108, 113, 16 and 9

hours after initial stage rise for Events 1, 2, 3, and 5, and also have steeper recovery curves with each successive event. Several studies have suggested a suppression of matrix flow in favor of conduit flow during storm events due to increased hydraulic head in conduits (Önder 1986; Goldscheider 2005, Wong et al. 2009). As antecedent conditions become more saturated the conduits may fill quicker after a storm and in effect act more efficiently to move stormwater. However, the physical arrangement and properties of the geologic system that is transmitting the water is not changing from event to event, which means that variable storage in different compartments in the unsaturated zone must be influencing flow and contributing to the changing signals over time.

Isotope data further supports shifting contributions from different storage components. Table 3 shows the ranges in $\delta^{18}O$ and $\delta^{2}H$ ratios across storm events. The range of values for a given storm response increased sharply in later events. This increase in the range of values is likely due to the increased efficiency that the system transited water during wet antecedent conditions. Also the majority of Main Stream samples from Event 1 plot along an evaporative trend line. This is likely because much of the Main Stream water in Event 1 is sourced from water in the soil and epikarst.

A leaky bucket conceptual of the different storage and flow components in a karst system similar to CWAN (Figure 17) illustrates with varying proportions of storage and different thicknesses of flowlines the probable evolution of storage and flow from the surface to Main Stream as antecedent conditions transition from wet to dry. As data from this study suggests, storage in the soil, epikarst, and vadose filled in Events 1 and 2. In subsequent events these storage compartments were bypassed in favor of more efficient transport via large fractures and conduits.

Tracer source concentrations

A conceptual model of a vertical cross section of CWAN (Figure 19) illustrates the source locations and concentrations of different tracers and how they vary within and across events with varying antecedent conditions. For example, the consistency in the overall behavior of DOC curves indicates water contribution to Main Stream from the soil and upper epikarst for all storm events. An explanation for the overall response differences of NO_3^-, Na^+, Cl^-, and SO_4^{2-} relative to DOC in Events 1 and 2 is likely because the soil and epikarst that concentrates these ions in the dry summer months were being flushed by precipitation in Events 1 and 2. Similarly, Mudarra et al. (2013) observed NO_3^- increases at springs in Malaga (southern Spain) during autumn recharge events only, and NO_3^-concentrations declined through the rest of the year during recharge events. Unlike these ions, DOC continues to concentrate in the soil as organic matter is degraded through the fall and winter months. Large concentrations of DOC are flushed from the soil through the karst system during Events 3-5, while relatively few NO_3^-, Na^+, Cl^-, and SO_4^{2-} ions remain in the soil to be flushed. Consequently these ions show overall dilution curves for Events 3-5 after autumn flushing.

NO_3^-, Na^+, Cl^-, and SO_4^{2-} continued to increase in concentration and DOC remained high in Main Stream at the end of Event 2 sampling, 15 days after the initial storm. 9 weeks later at the start of Event 3, initial concentrations of NO_3^-, Na^+, Cl^-, and SO_4^{2-} are higher than the peak concentrations in Event 2. These waters with relatively high NO_3^-, Na^+, Cl^-, and SO_4^{2-} are likely waters remaining from Events 1 and 2 that were still moving through the system at the onset of Event 3. DOC and SC have low and high values respectively and are indicative of older water, not relatively recent stormwater.

These older water signatures in DOC and SC are likely due to the non-conservative nature of DOC and SC over the 9 weeks between storms. Figure shows the relationship between, DOC, Mg^{2+}, NO_3^-, Cl^-, and event/pre-event water totals for Events 1, 2, 3 and 5.

Isotope data further supports a cyclical flushing of water through CWAN. Figure 14 shows the majority of samples (50 of 91) from Event 1 plot on an evaporitic trend away from the GMWL, indicating these waters had$\delta^{18}O/\delta^{2}H$ ratios indicative of evaporative fractionation. It is likely that during Event 1 a large amount of water was flushed from and through the shallow soil and epikarst, where it had been subjected to evaporative losses and isotopic fractionation, especially after a dry, hot summer.

Sediment

Recent studies have highlighted the susceptibility of karst systems to large sediment fluxes during storm events (Klimchouk 2004, Williams 2008). Storm events mobilize sediments that act as reservoirs for various contaminants and metals (Mahler et al. 2000; Vesper and White 2003). Also recent studies have distinguished two distinct turbidity peaks, first pulse-through turbidity from re-suspension of autochthonous sediment followed by flow-through turbidity of allochthonous sediment have been documented in several studies (Massei et al. 2003; Pronk et al. 2009; Goldscheider et al. 2010). TSS and NVSS peak times were significantly correlated with conductivity minimum times. This gives a clue that sediment flux through CWAN is likely more dependent on allochthonous input from stormwater than from resuspension of sediment in the cave. This is consistent with results from Barton Springs in Austin Texas (Mahler and Lynch 1999.) Maximum sediment concentrations were not significantly correlated with any antecedent environmental predictors or rainfall predictors. This is not surprising

as sediment transport likely depends on a number of factors which could not be modeled given the limited number of storm events.

V. CONCLUSIONS

The analysis of data representing a large number of natural environmental tracers at frequent time intervals over five storm events with differing seasons and antecedent conditions has given insight into kart recharge processes. This study highlights the complexities in interpreting data from different tracers, and shows that it may be impossible to physically characterize a karstic hydrologic system from one or even a few storm events. As antecedent conditions transitioned from dry to wet, peak event water moved through CWAN on time scales from several days to only hours. Dissolved and particulate loads varied in concentration within and across multiple storm events. These differences depended on the antecedent conditions, which also affected evolving storage components and flow paths as well as changing source concentrations through time. This study highlights the caution that must be taken when analyzing a system based on few tracers as infiltrating surface water and groundwater may have varying concentrations of natural tracers and display quite different behaviors across different hydrographs. All of these factors must be considered in any hydrologic model of similar karst systems.

Figure 1. Location of CWAN (blue dot) relative to the Trinity Formation (modified from Clarke et al. 2014).

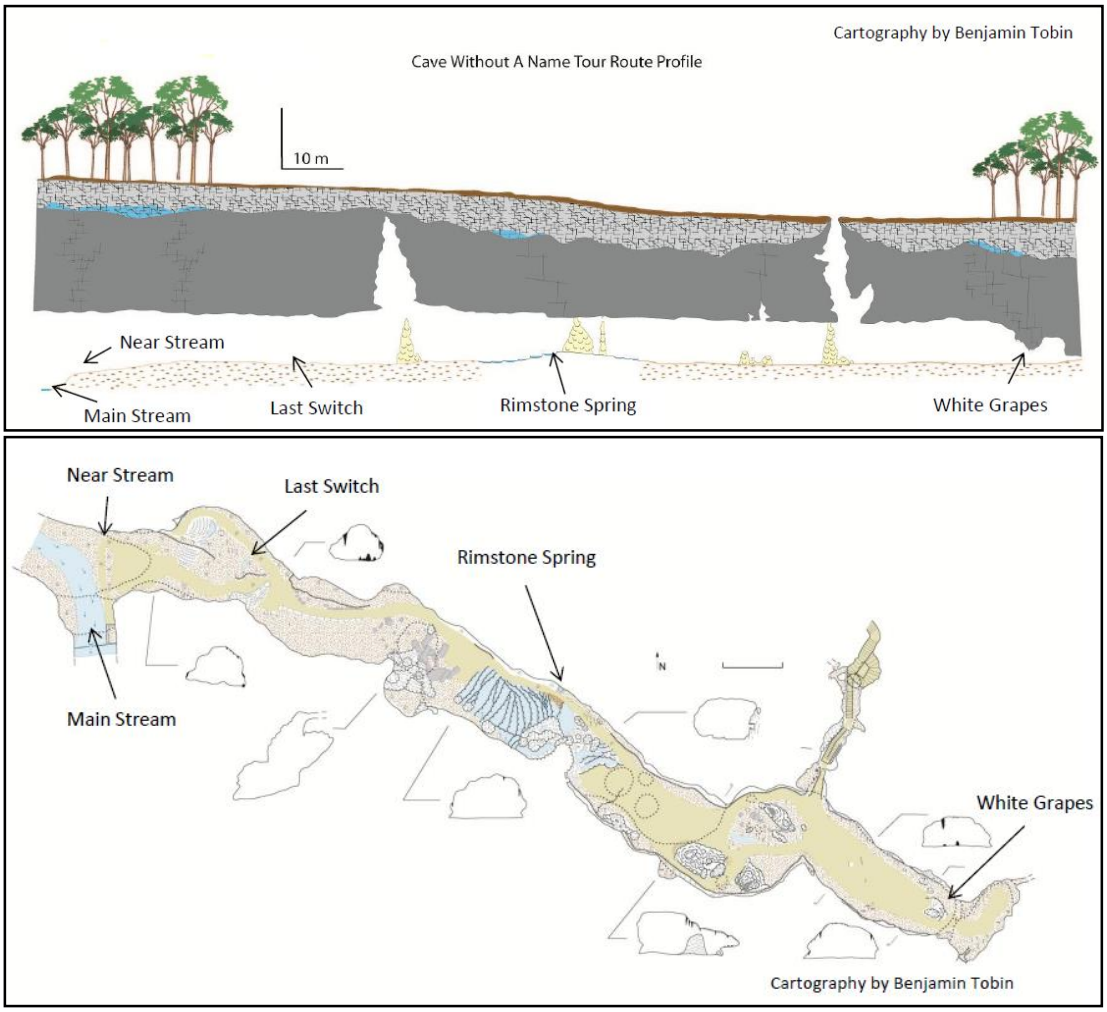

Figure 2. Vertical (top) and horizontal (bottom) cross sectional view of the commercial section of CWAN with five permanent monitoring sites.

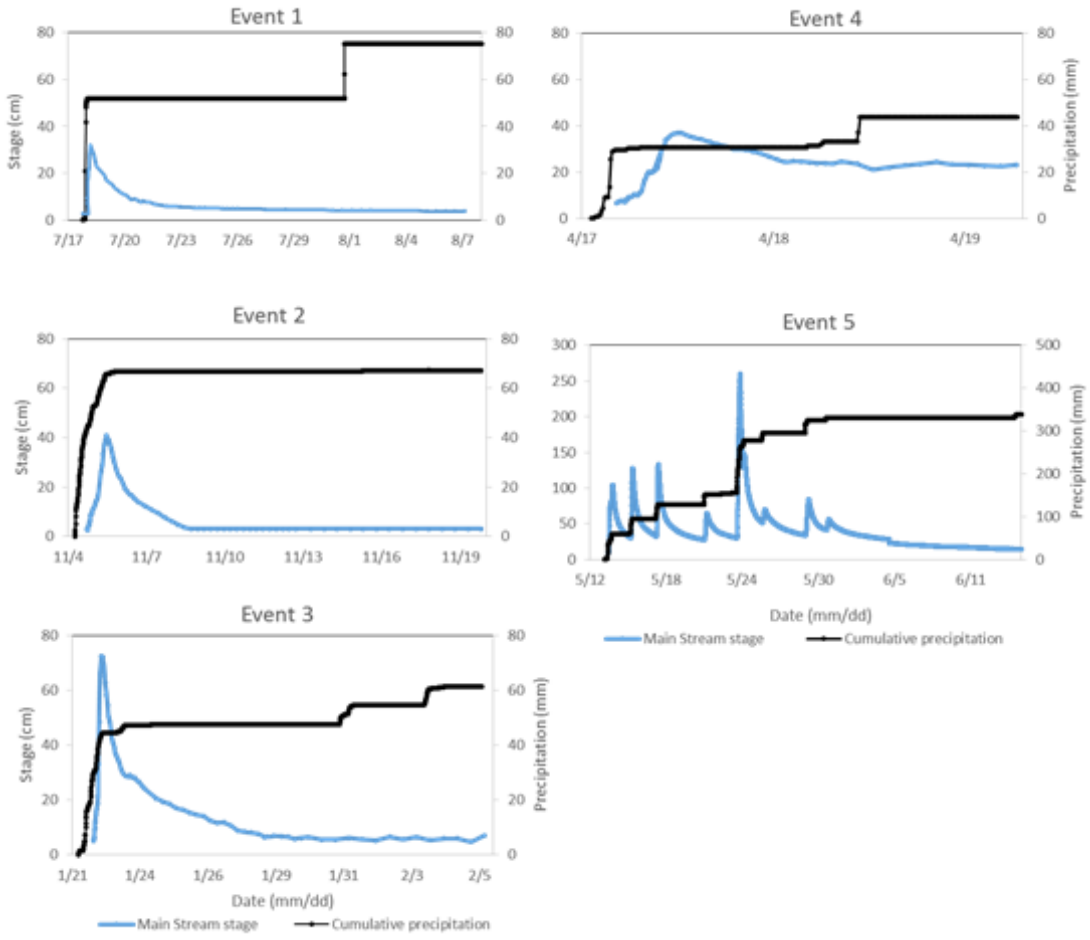

Figure 3. Cumulative precipitation (mm) and Main Stream Stage response for Events 1-5.

Event	Initial surface runoff to initial stage rise	Initial stage rise to stage peak
1	2:31	4:15
2	10:26	17:40
3	8:42	7:00
4	1:22	7:09
5	1:10	9:00

Table 1. Compares lags from initial surface runoff to initial Main Stream Stage response and Main Stream stage peak.

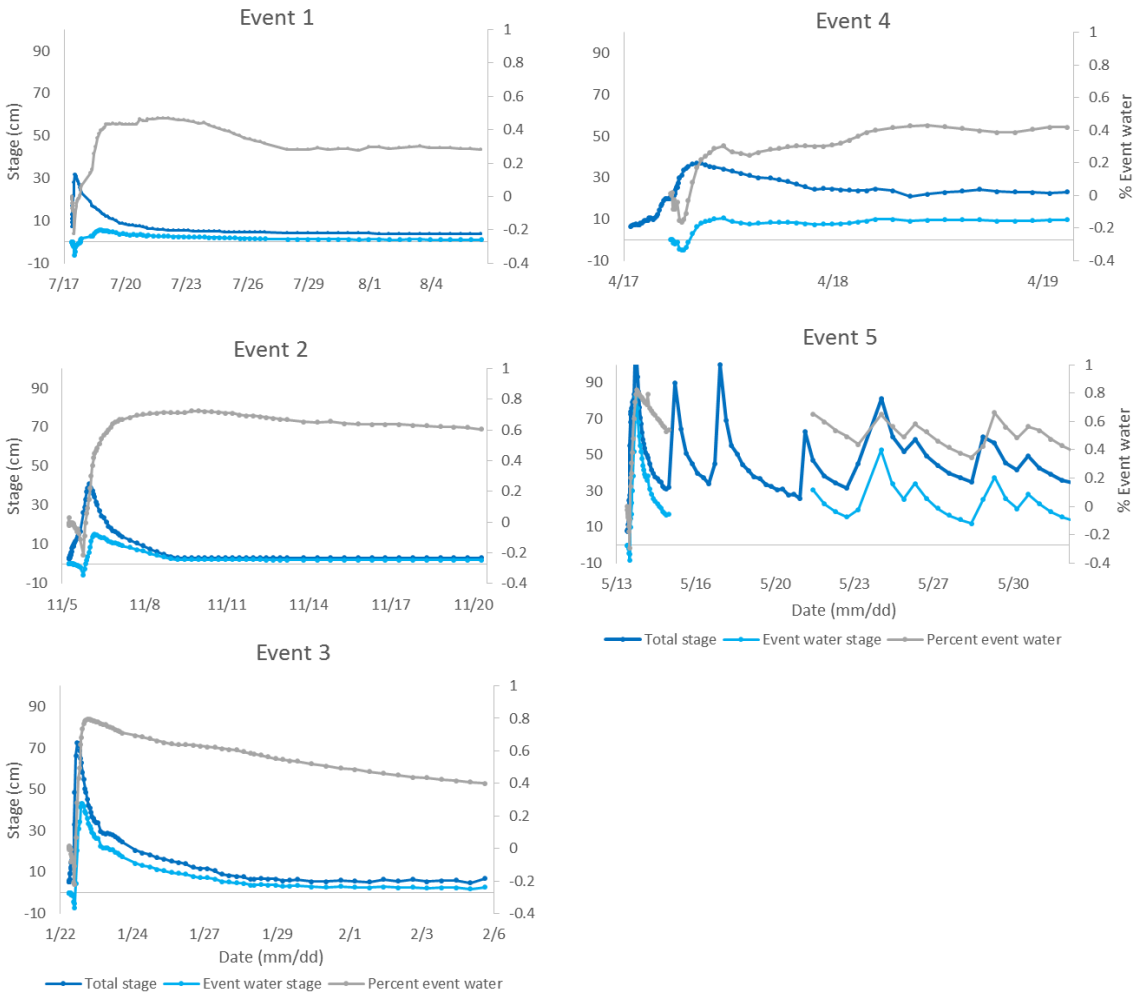

Figure 4. Hydrograph separation analysis using a two end-member mixing model of Mg^{2+} concentrations, and shows percent event water and Main Stream stage, and event water stage height (cm).

Event	Initial stage rise to stage peak	Initial stage rise to event water peak %
1	4:15	107:44
2	17:40	113:20
3	7:00	16:24
4	7:09	10:39
5	9:00	9:25

Table 2. Compares lags from initial Main Stream response to stage peak and event water percentage peak.

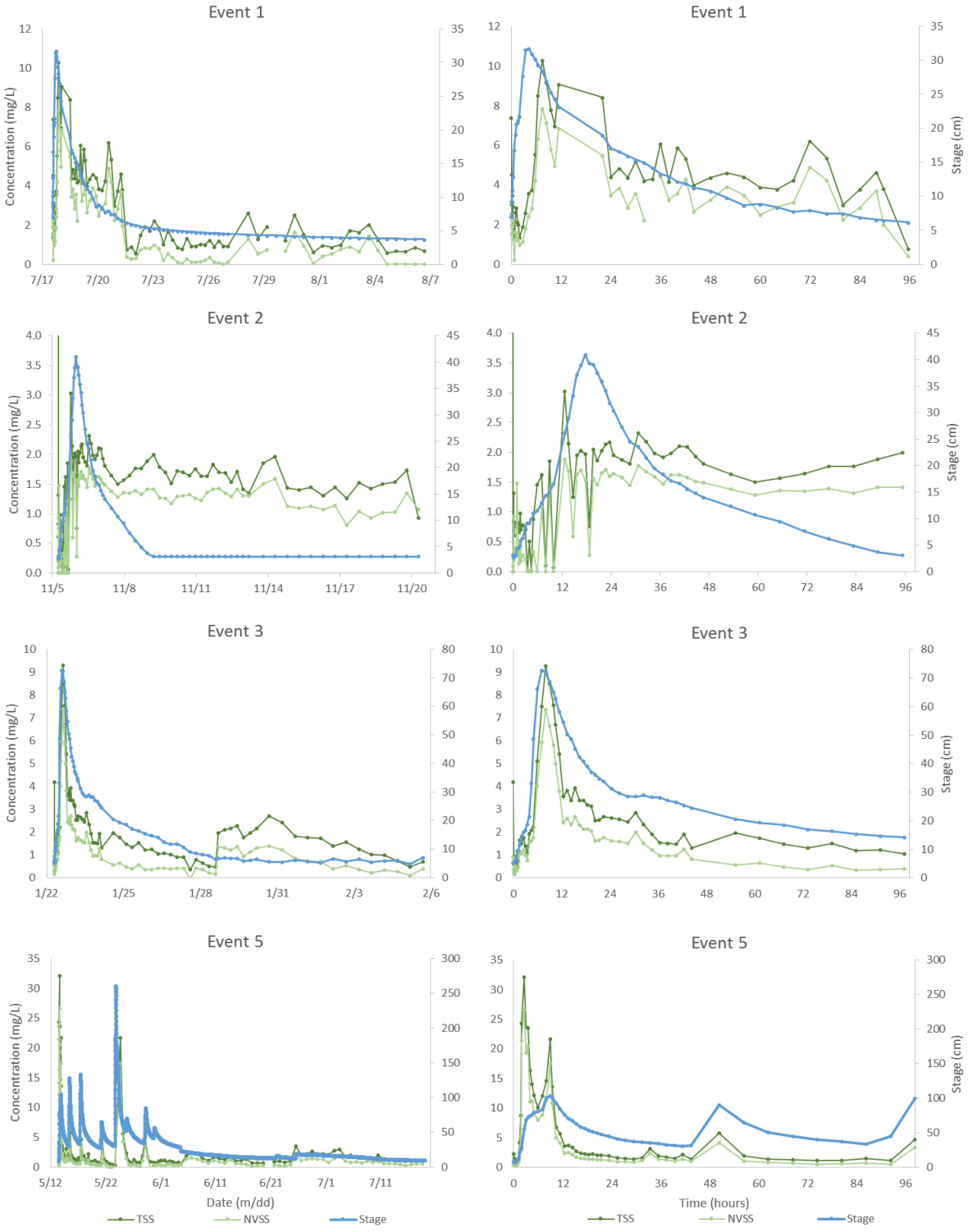

Figure 5. TSS, NVSS and Main Stream stage for Events 1, 2, 3 and 5. Left side shows entire sampling period, right side shows first 96 hours of sampling period.

Figure 6. TP, SRP and Main Stream stage for Events 1, 2, 3 and 5. Left side shows entire event, right side shows first 96 hours of sampling period.

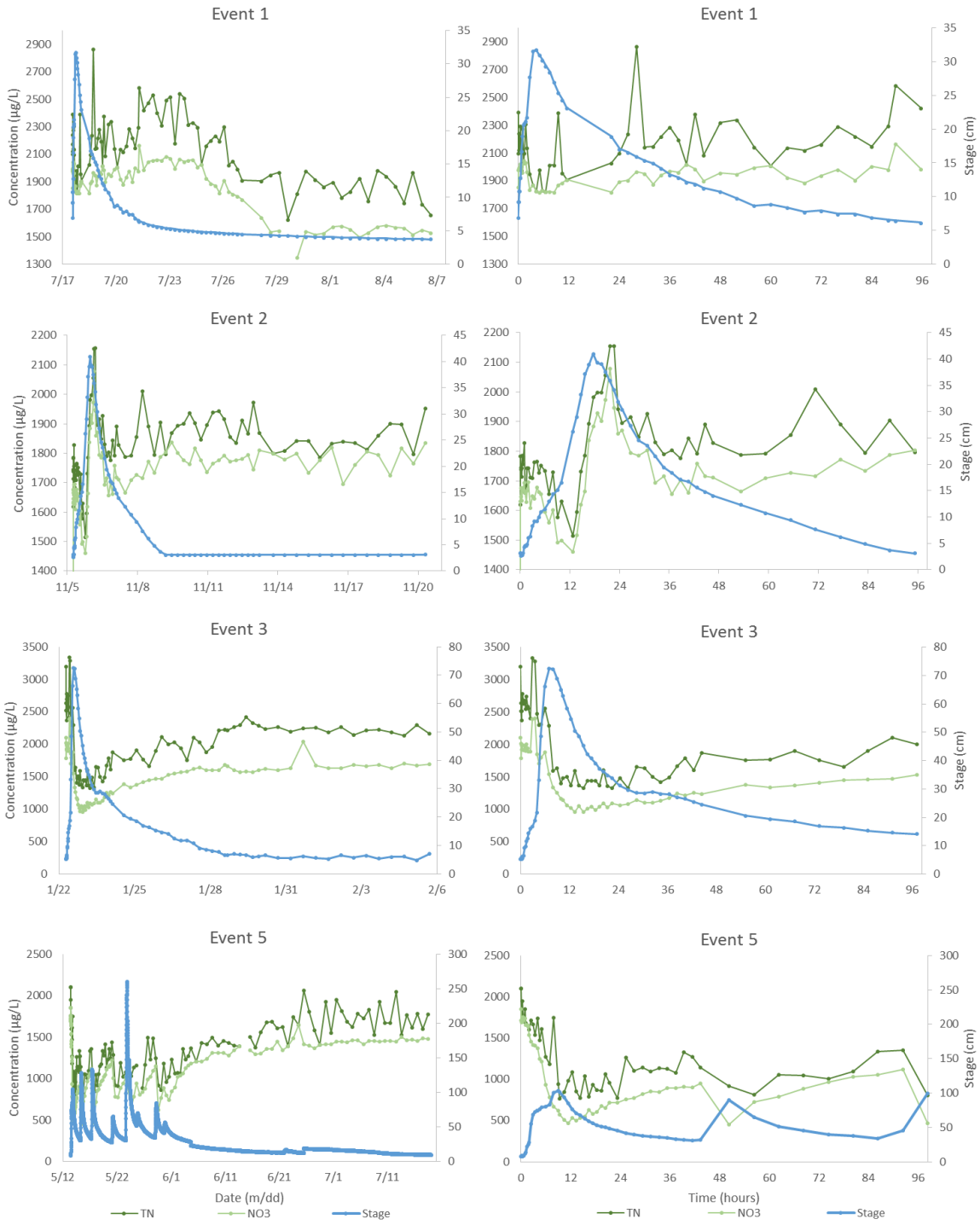

Figure 7. TN, NO_3^- and Main Stream stage for Events 1, 2, 3 and 5. Left side shows entire sampling period, right side shows first 96 hours of sampling period.

Figure 8. DOC, NH_4 and Main Stream stage for Events 1, 2, 3 and 5. Left side shows entire sampling period, right side shows first 96 hours of sampling period.

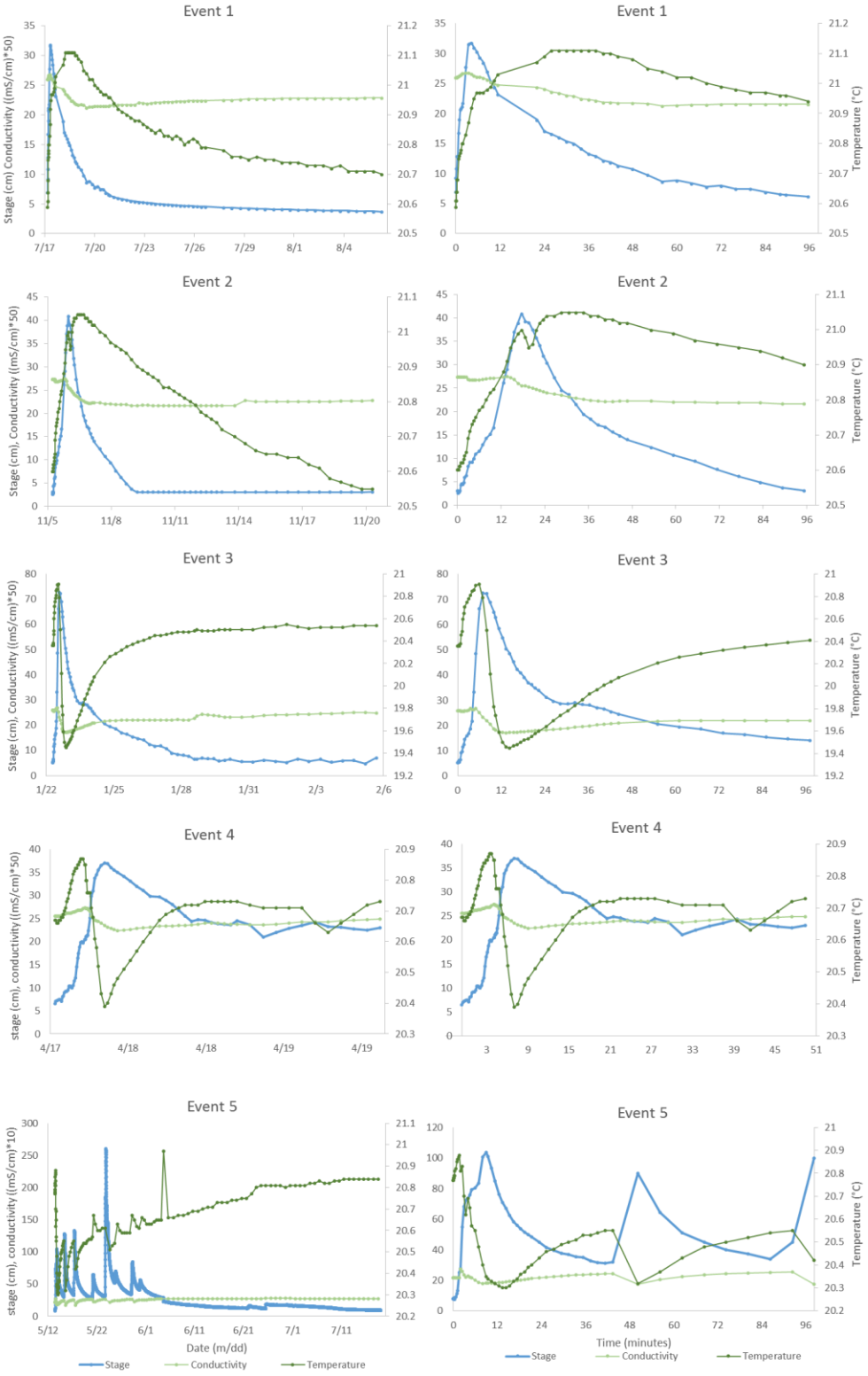

Figure 9**.** Temperature, electrical conductivity and Main Stream stage for Events 1-5. Left side shows entire sampling period, right side shows first 96 hours of sampling period.

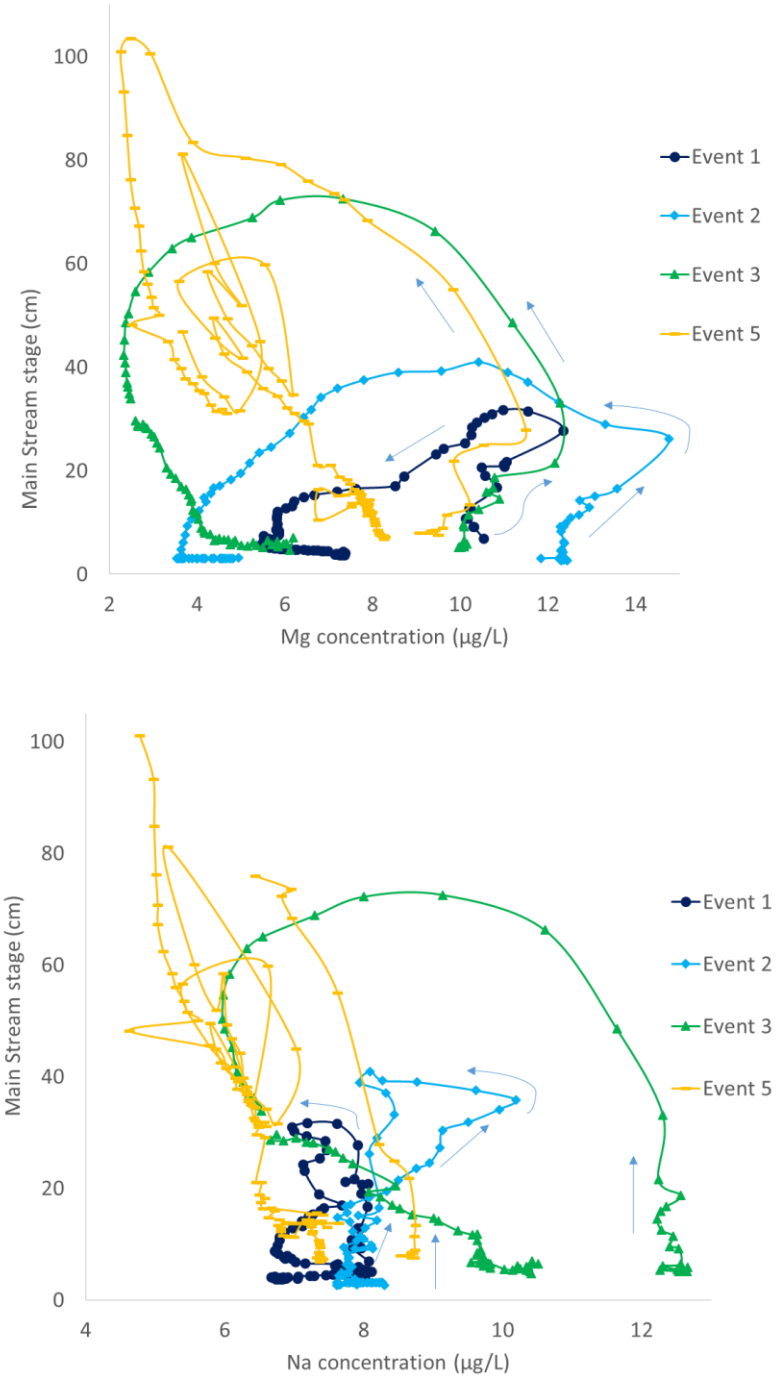

Figure 10. Hysteresis plots of Mg^{2+} and Na^{2+} ion concentrations for Events 1, 2, 3 and 5.

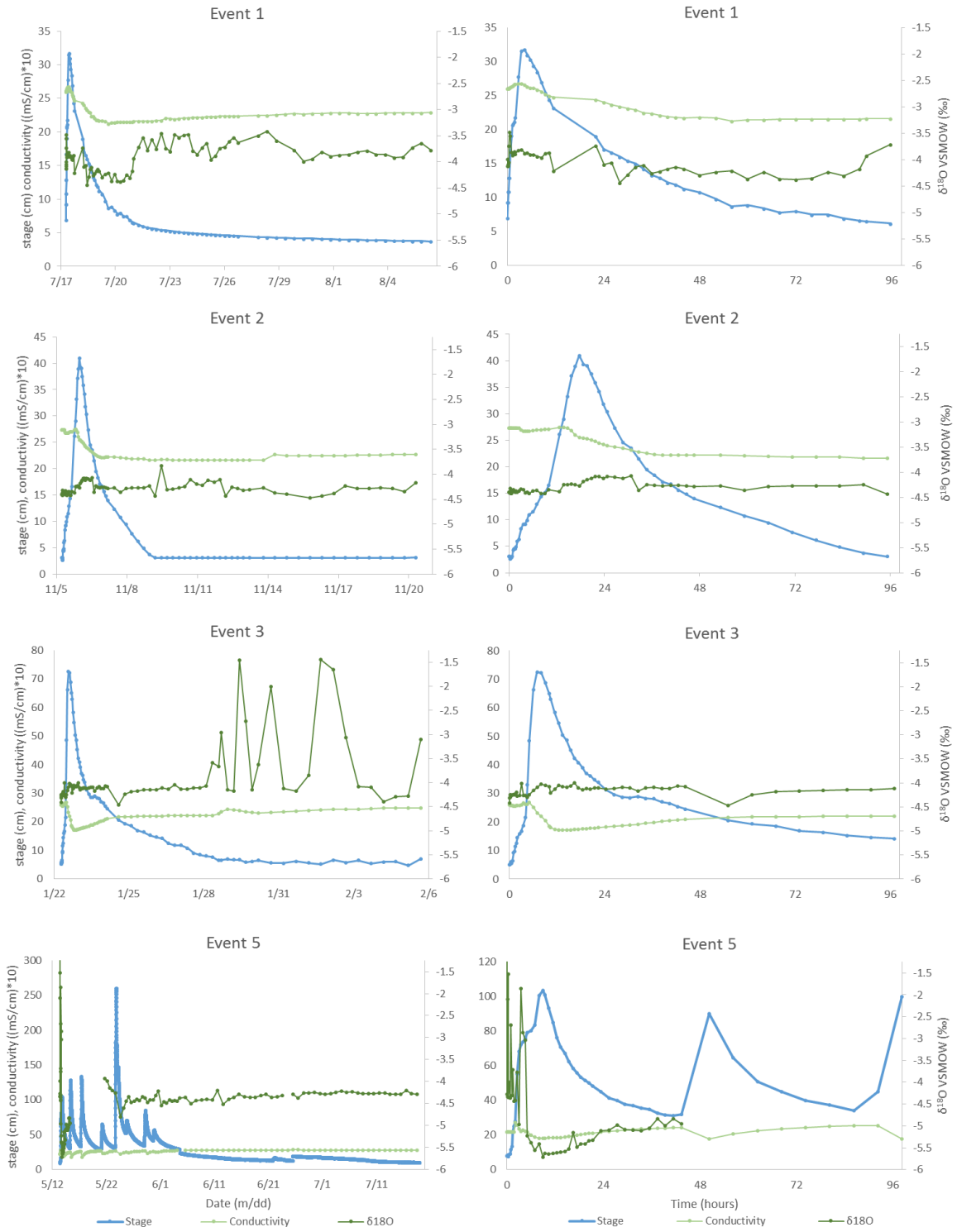

Figure 11. $\delta^{18}O$ ratio, conductivity, and Main Stream stage for Events 1, 2, 3 and 5. Left side shows entire sampling period, right side shows first 96 hours of sampling period.

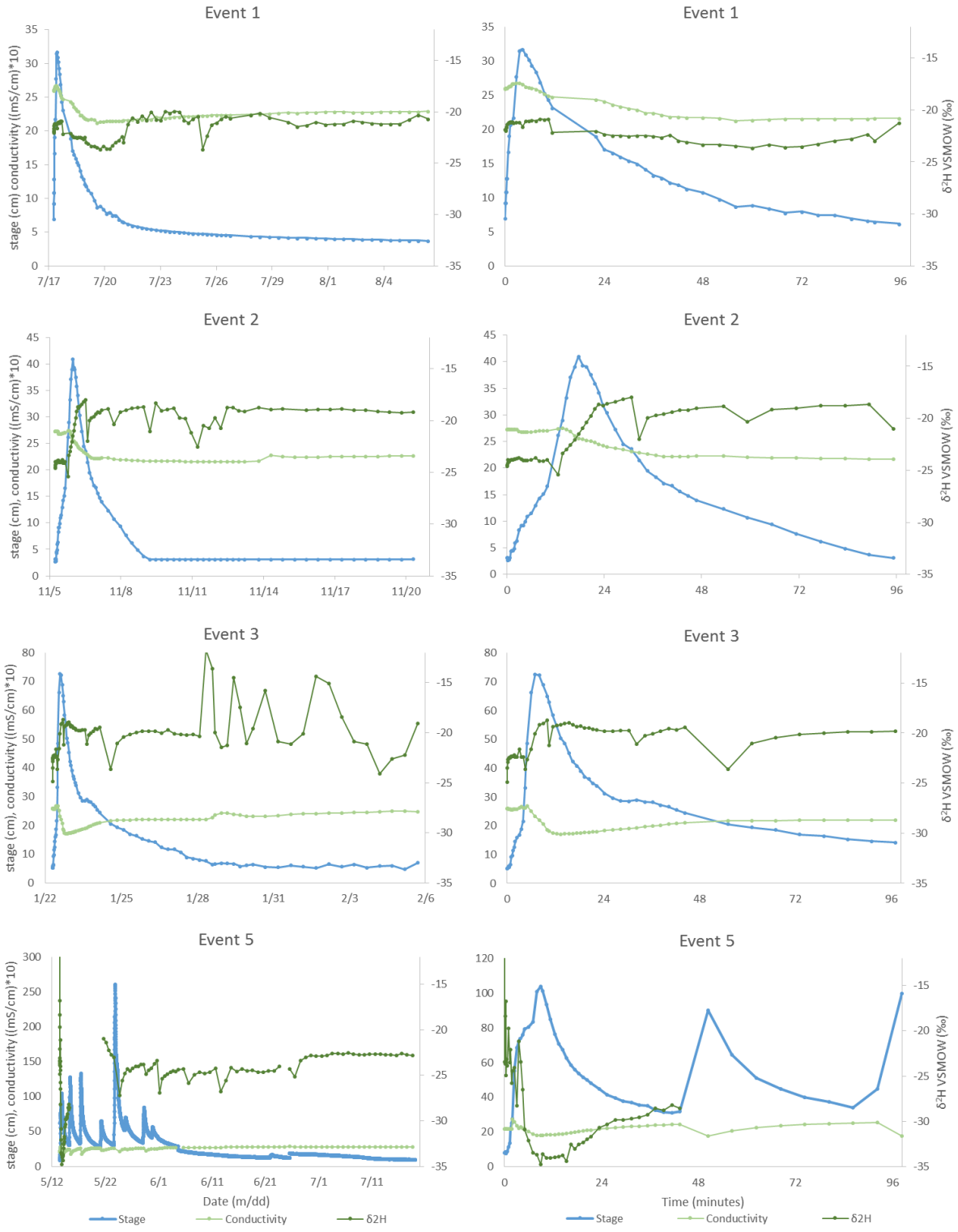

Figure 12. δ^2H ratio, conductivity, and Main Stream stage for Events 1, 2, 3 and 5. Left side shows entire sampling period, right side shows first 96 hours of sampling period.

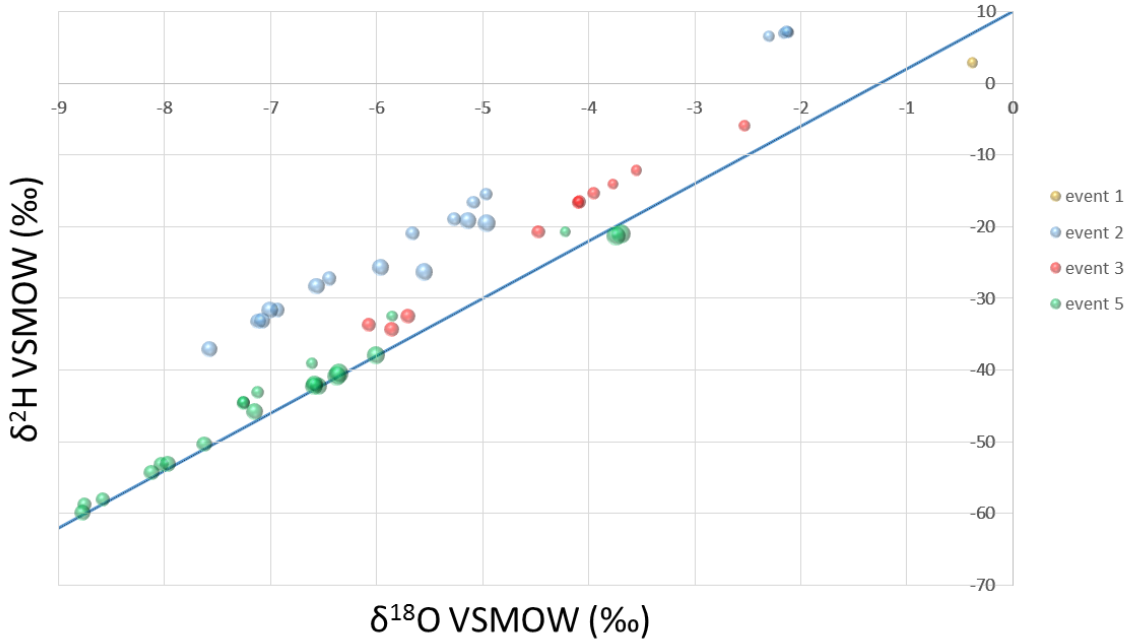

Figure 13. δ^2H vs $\delta^{18}O$ for surface runoff samples (Events 1, 2, 3 and 5). GMLW is shown as solid blue line.

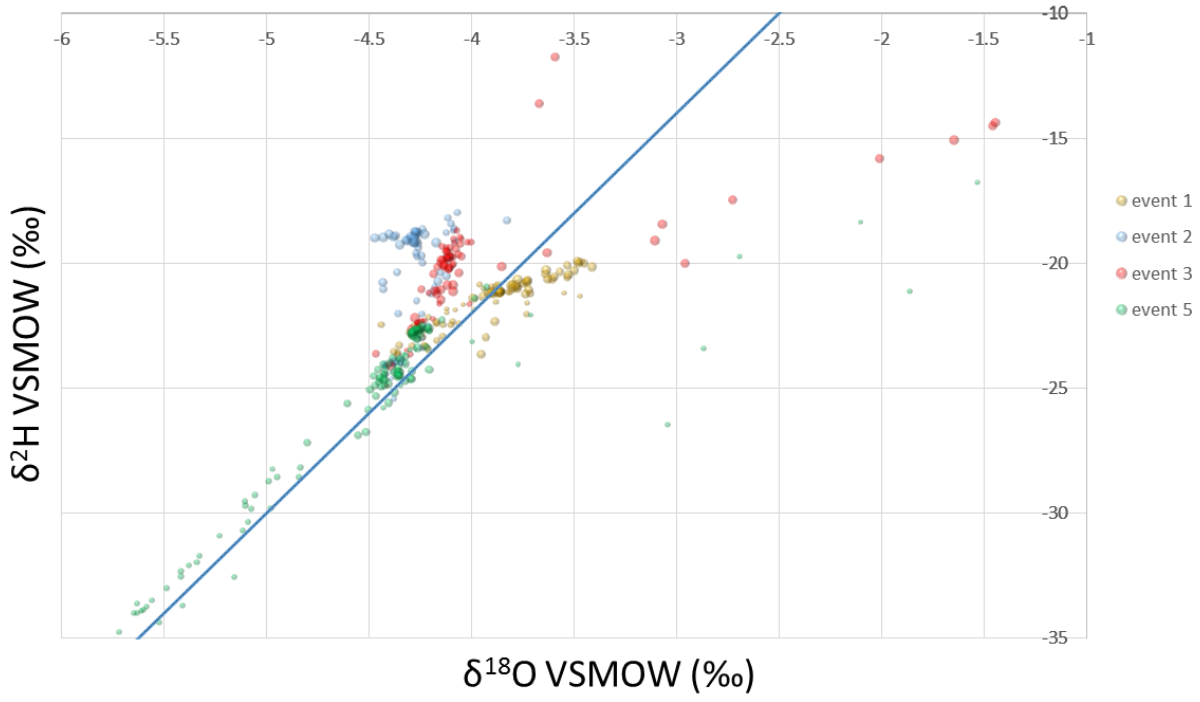

Figure 14. δ^2H vs $\delta^{18}O$ for Main Stream samples (Events 1, 2, 3, and 5). GMLW is shown as solid blue line.

	$\delta^{18}O$ VSMOW (‰)			$\delta^{2}D$ VSMOW (‰)		
	Maximum	Minimum	Difference	Maximum	Minimum	Difference
Event 1	-3.41	-4.44	1.03	-19.92	-23.66	3.74
Event 2	-3.83	-4.47	0.64	-17.97	-25.43	7.46
Event 3	-1.44	-4.47	3.02	-11.77	-24.89	13.12
Event 5	2.10	-5.72	7.82	-7.66	-34.76	27.10

Table 3. Range of $\delta^{2}H$ and $\delta^{18}O$ ratios in Main Stream (left) and surface runoff (right) for Events 1, 2, 3, and 5.

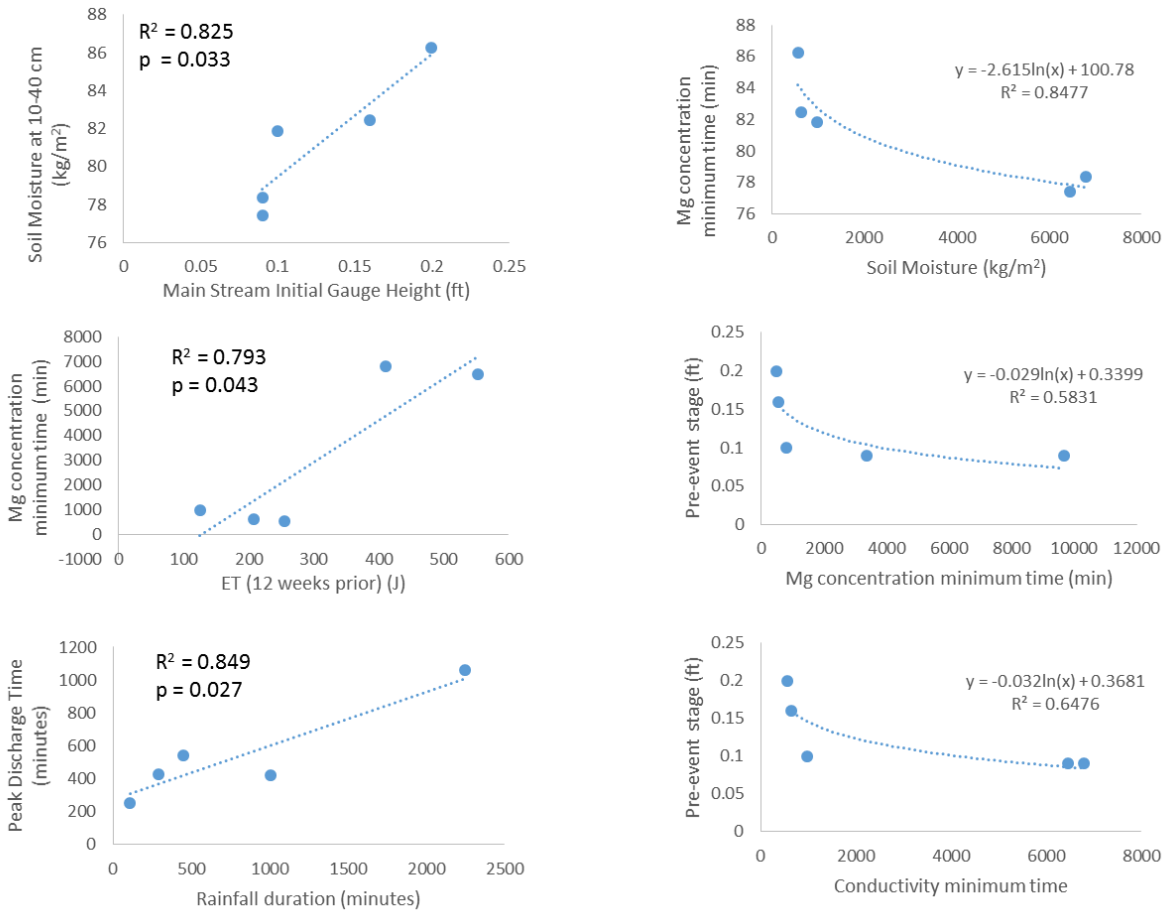

Figure 15. Relationships between various environmental parameters across the five storm events.

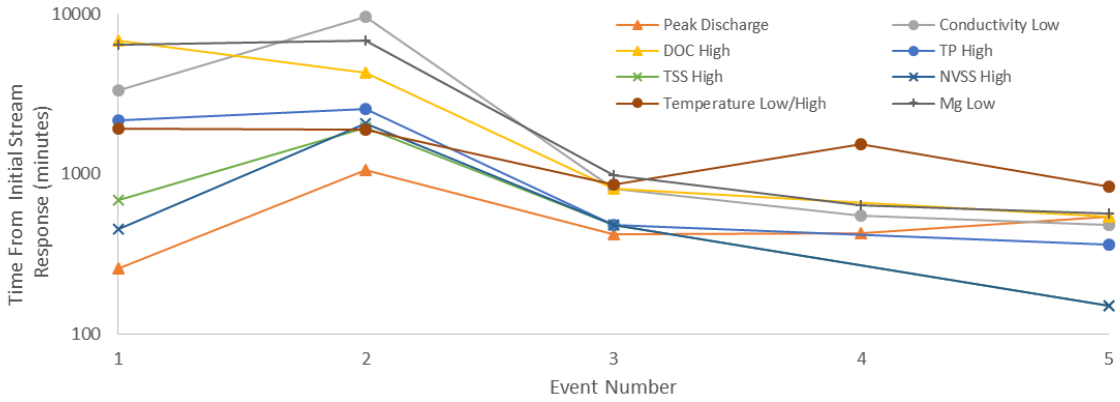

Figure 16. Relative timing of maximum or minimum values for select tracers for each event. Vertical axis is log-scale in minutes since initial increase in stage at the Main Stream site.

Event 1		Event 2		Event 3		Event 4		Event 5	
Discharge	4:15	Discharge	17:40	Discharge	7:00	Discharge	7:09	TSS	2:30
NVSS	7:30	Temperature	31:40	TSS	8:00	Conductivity	9:09	NVSS	2:30
TSS	11:30	TSS	32:40	NVSS	8:00	Mg	10:39	TP	6:00
Temperature	32:04	NVSS	34:40	TP	8:00	Temperature	25:36	Conductivity	8:00
TP	36.04	TP	42:40	DOC	13:24			Discharge	9:00
Conductivity	56:04	DOC	71:20	Conductivity	13:24			DOC	9:00
Mg	107:44	Mg	113:20	Temperature	14:24			Mg	9:25
DOC	113:44	Conductivity	161:20	Mg	16:24			Temperature	13:55

Table 4. Timing of minimum or maximum values (hours: minutes) for select tracers relative to initial Main Stream response. These data are shown in graph-format in Figure 15.

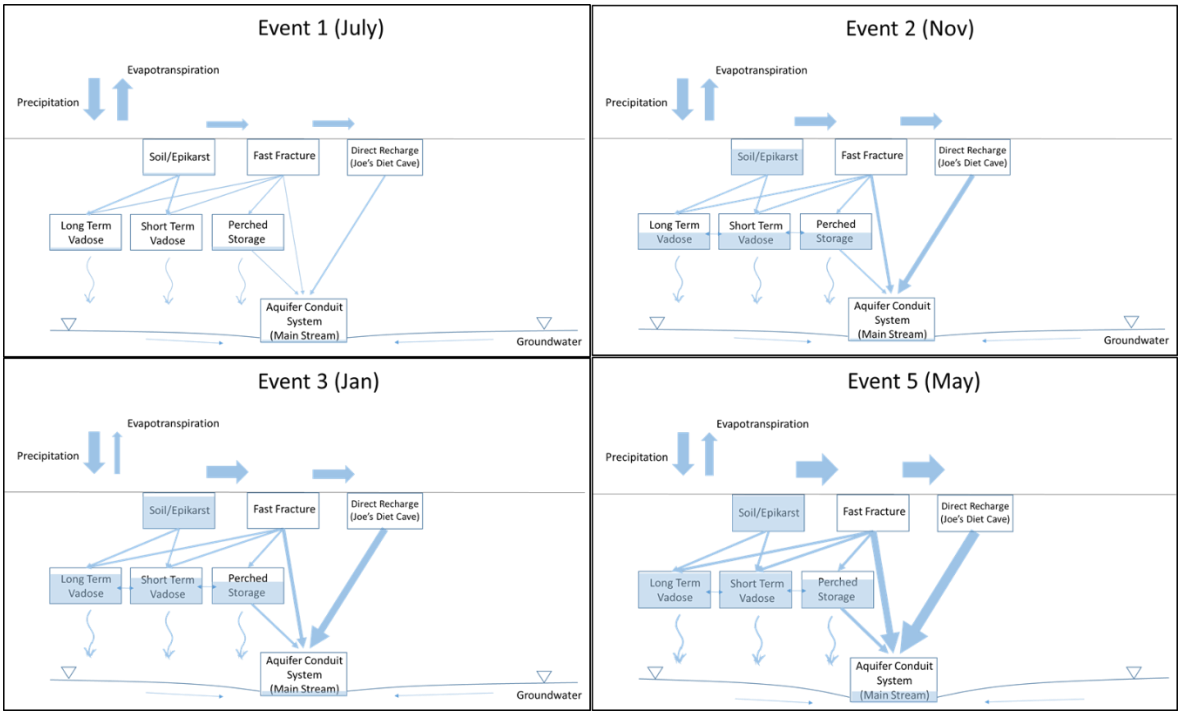

Figure 17. Leaky bucket conceptual model showing changes in storage and flow paths across events as the system moves from dry to wet antecedent conditions.

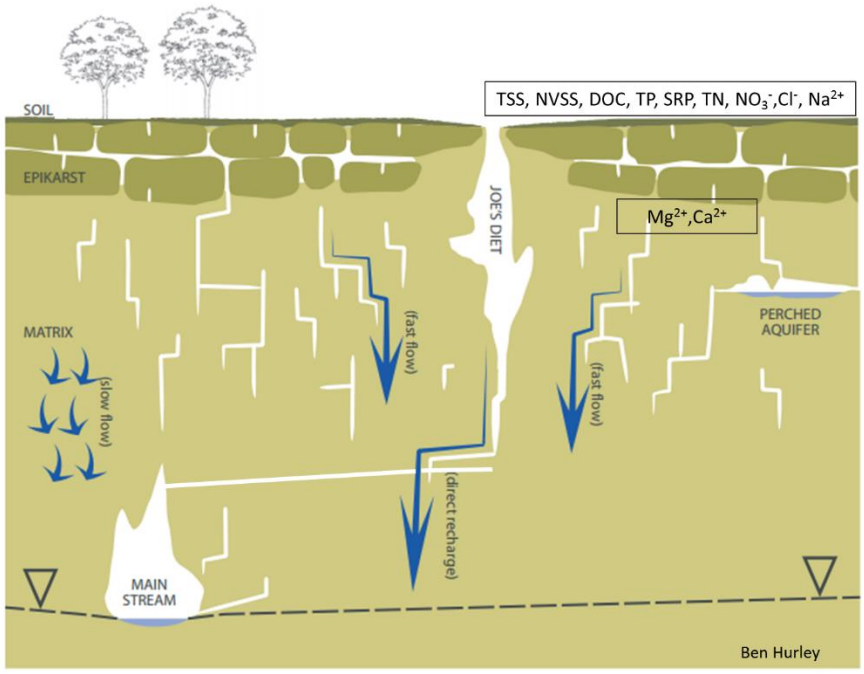

Figure 18. A conceptual vertical cross section of the karst system at CWAN with the source locations of different tracers.

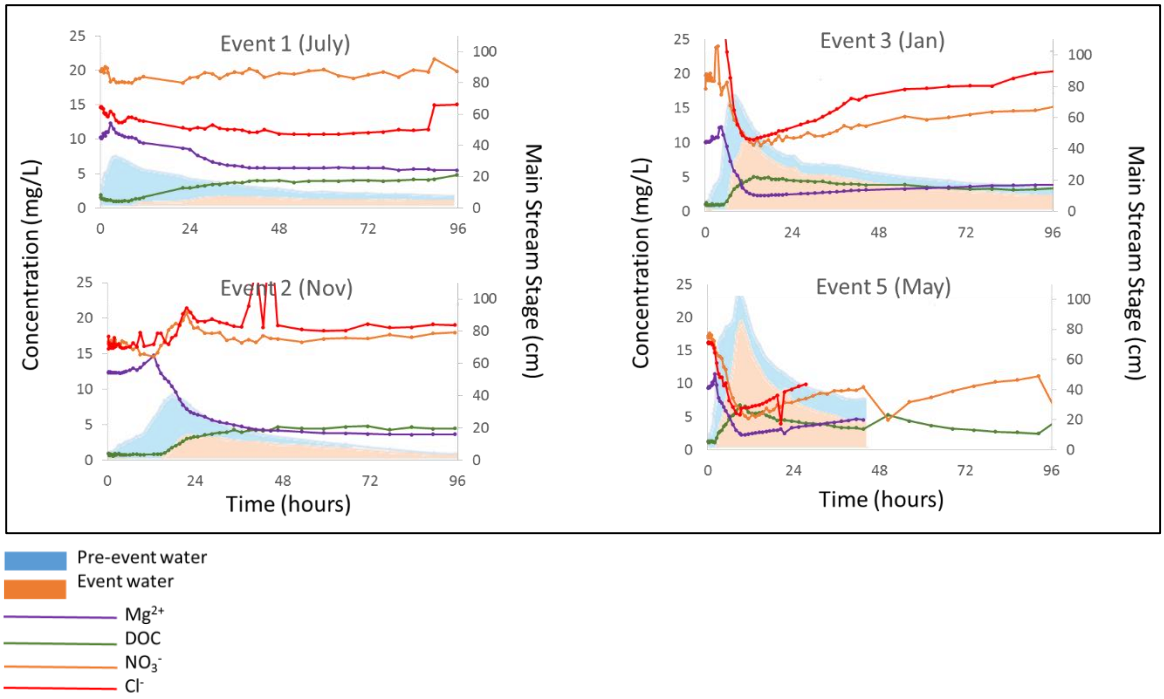

Figure 19. Tracer concentrations within and across Events 1, 2, 3, and 5 with event and pre-event ratios.

REFERENCES

Allen, R. G. 2005. The ASCE Standardized Reference Evapotranspiration Equation. American Society of Civil Engineers.

Batiot, C. 2002. Étude expérimentale du cycle du carbone en régions karstiques. Apport du carbone organique et du carbone minéral à la connaissance hydrogéologique des systèmes. PhD thesis, University of Avignon, Avignon, France.

Blavoux, B. 1978. Etude du cycle de l'eau au moyen de l'oxygène 18 et du tritium, Univ. Pierre et Marie Curie, Paris, 333.

Chloet, C., M. Steinmann, J.B. Charlier, and S. Denimal. 2015. Comparative Study of the Physiochemical Response of Two Karst Systems During Contrasting Flood Events in the French Jura Mountains. Hydrogeological and Environmental Investigations in Karst Systems. Environmental Earth Sciences 1, 1-9.

Clark, B.R., J.R. Bumgarner, N.A. Houston, and A.L. Foster. 2014. Simulation of groundwater flow in the Edwards-Trinity and related aquifers in the Pecos County region, Texas. U.S. Geological Survey Scientific Investigations Report 56: 2013–5228.

Cleveland, W.S., and S.J. Devlin. 1988. Locally Weighted Regression: An Approach to Regression Analysis by Local Fitting. Journal of the American Statistical Association 83: 596-610.

Crumpton, W.G., T.M. Isenhart, and P.D. Mtchell. 1992. Nitrate and organic N analysis with second-derivative spectroscopy. Limnology and Oceanography 22: 760-764.

Dansgaard, W. 1964. Stable isotopes in precipitation. Tellus 16, 436-468.

Doctor D.H., E.C. Alexander Jr, M. Petrič, J. Kogovšek, J. Urbanc, S. Lojen, and W. Stichler, 2006. Quantification of karst aquifer discharge components during storm events through end-member mixing analysis using natural chemistry and stable isotopes as tracers. Hydrogeology Journal 14, 7: 1171-1191.

Dreiss, S.J. 1989. Regional Scale Transport in a Karst Aquifer 1. Component Separation of Spring Flow Hydrographs. Water Resources Research 25: 117-125.

Ford, D.C., and P.W. Williams, 2007. Karst hydrogeology and geomorphology. Wiley, Chichester.

Fournier M, N. Massei, M. Bakalowicz, L. Dussart-Baptista, L. Rodet, and J.P. Dupont. 2007. Using turbidity dynamics and geochemical variability as a tool for understanding the behavior and vulnerability of karst aquifer. Hydrogeology Journal 15, 4: 689–704.

Gerard, B. 2012. Effects of Environmental Parameters and Precipitation Dynamics on Infiltration and Recharge into the Trinity Aquifer of Central Texas. Department of Biology. San Marcos, Texas State University. M.S. 17-18.

Goldscheider, N. 2005. Fold structure and underground drainage pattern in the alpine karst system Hochifen-Gottesacker. Eclogae Geologicae Helvetiae 98, 1: 1–17.

Goldscheider, N., M. Pronk, and J. Zopfi. 2010. New Insights into the transport of sediments and microorganisms in Karst groundwater by continuous monitoring of particle-size distribution. Geologia Croatica 63, 2: 137-142.

Hawes, R.S. 1939. The Flood Factor in the Ecology of Caves. Journal of Animal Ecology 8, 1:1-5.

Klimchouk, A. 2004. Towards Defining, Delimiting, and Classifying Epikarst: Its Origin, Processes and Variants of Geomorphic Evolution. Speleogenesis and Evolution of Karst Aquifers 2, 1: 1–13.

Mace, R. E., A. H. Chowdhury, R. Anaya, and S.C. Way. 2000. Groundwater Availability of the Trinity Aquifer, Hill Country Area, Texas: Numerical Simulations Through 2050. Texas Water Development Board Report 353: 119.

Mahler, B.J., and Lynch, F.L. 1999. Muddy waters: Temporal variation in sediment discharging from a karst spring. Journal of Hydrology 214: 165-178.

Mahler, B.J., J.C. Personne, G.F. Lods, and C. Drogue. 2000. Transport of free and particulate-associated bacteria in karst. Journal of Hydrology 238, 3–4: 179–193.

Mahler, B.J., and Garner, B.D. 2009. Using nitrate to quantity quick flow in a karst aquifer. Ground Water 47, 350-360.

Martin, J.B., and R.W. Dean. 1999. Temperature as a natural tracer of short residence times for groundwater in karst aquifers, in A.N. Palmer, M.V. Palmer, and I.D. Sasowsky, Karst Modeling. Karst Waters Institute Special Publications 5: 236-242.

Massei, N., H.Q. Wang, J.P. Dupont, J. Rodet, and B. Laignel. 2003. Assessment of direct transfer and resuspension of particles during turbid floods at a karstic spring. Journal of Hydrogeology 275, 109-121.

Mudarra, M., and Andreo, B. 2013. Hydrochemical dynamics of TOC and NO_3^- contents as natural tracers of infiltration in karst aquifers. Environmental Earth Sciences 71, 2: 507-523.

NASA. 2015. Global Change Master Directory: Discover Earth Science Data and Services. gcmd.gsfc.nasa.gov.

NOAA. 2012. San Antonio Climate Summary. National Weather Service Weather Forecast Office.

Önder, H. 1986. Interaction between conduit type flow and diffuse flow in karst formations. IAHS-AISH 161, 371–385.

Pape, J.R., J.L. Banner, L.E. Mack, M. Musgrove, and A. Guilfoyle.2010. Controls on oxygen isotope variability in precipitation and cave drip waters, central Texas, USA. Journal of Hydrology 385, 203-215.

Perrin, K., P.Y Jeannin, and F. Zwahlen. 2003. Epikarst storage in a karst aquifer: a conceptual model based on isotopic data, Milandre test site, Switzerland. Journal of Hydrology 279, 106–124.

Perrin, J., P.Y. Jeannin, and F. Cornaton. 2007. The role of tributary mixing in chemical variations at a karst spring, Milandre, Switzerland. Journal of Hydrology 332, 152–173.

Polk, J. S., S. Vanderhoff, C. Groves, B. Miller, and C. Bolster. 2013. Complex epikarst hydrogeology and contaminant transport in a southcentral Kentucky karst landscape, in proceedings of the 16th International Congress of Speleology, Brno, Czeck Republic 110-115.

Pronk, M., N. Goldscheider, J. Zopfi, and F. Zwahlen. 2009. Percolatioin and particle transport in the unsaturated zone of a karst aquifer. Ground Water 47, 3: 361-369.

R Core Team, 2015. R: A language and environment for statistical computing. R Foundation for Statistical Computing, Vienna Austria. URL http://www.R-project.org/.

Ryder, P.D. 1996. Ground water atlas of the United States, Oklahoma, Texas. U.S Geological Survey, HA 730-E.

Standard Methods Online. Standard Methods for the Examination of Water and Wastewater. http://standardmethods.org.

Shuster, E.T., and White W.B. 1971. Seasonal fluctuations in the chemistry of limestone springs: A possible means for characterizing carbonate aquifers. Journal of Hydrogeology 14: 93-128.

Schwartz, B.F, S. Schwinning, B. Gerard, K.R. Kukoski, C.L. Stinson, and H.C. Dammeyer. 2013. Using hydrogeochemical and ecohydrologic responses to understand epikarst process in semi-arid systems, Edawards Plateu, Texas, USA. Acta Carsologica 42: 315-325.

Thomas, R.B., and R.E. Eads. 1983. Contamination of Successive Samples in Portable Pumping Systems. Water Resources Research 19, 2:436-440.

Toran, L., and C.E. Reisch. 2012. Using stormwater hysteresis tocharacterize karst spring discharge. Groundwater 15: 575-587.

Toran, L., and W.B. White. 2005. Variation in nitrate and calcium as indicators of recharge pathways in Noolte Spring, PA. Environmental Geology 48: 854-860.

Toran, L., J.H. Tancredi, E.K. Herman, and W.B. White. 2006. Conductivity and sediment variation during storms as evidence of pathways in karst springs, in Harmon, R.S., and Wicks, C., eds., Perspectives on karst geomorphology, hydrology, and geochemistry – A tribute volume to Derek C. Ford and William B. White.Geological Society of America Special Paper 404: 169-176.

Vanderhoff, S.M. 2011 Multiple Stom Event Impaccts on Epikarst Storage and Transport of Organic Soil Amendments in South-Central Kentucky. Department of Geography and Geology. Western Kentucky University. M.S.

Veni, G. 1994. Geomorphology, Hydrogeology, Geochemistry, and Evolution of the Karstic Lower Glen Rose Aquifer, South-central Texas. Pennslvania State University.

Vesper, D.J., and W.B. White. 2003. Metal transport to karst springs during storm flow: An example from Fort Camp-bell, Kentucky/Tennessee, USA. Journal of Hydrology 276, 1–4: 20–36.

Wetzel, R.G., and G. Likens, 2000. Limnological Analyses, Third Edition. 87-88.

Wong, C.I., B.J. Mahler, M. Musgrove, and J.L. Banner. 2012. Changes in sources and storage in a karst aquifer during a transition from drought to wet conditions. Journal of Hydrology 468: 159-172.

White, W.B. 1988. Geomorphology and Hydrology of Karst Terrains. New York: Oxford University Press.

Yang, P., D. Yuan, X. Ye, S. Xie, X. Chen, and Z. Liu. 2013. Sources and migration path of chemical compositions in a karst groundwater system during rainfall events. Chinese Science Bulletin 58, 2488–2496.